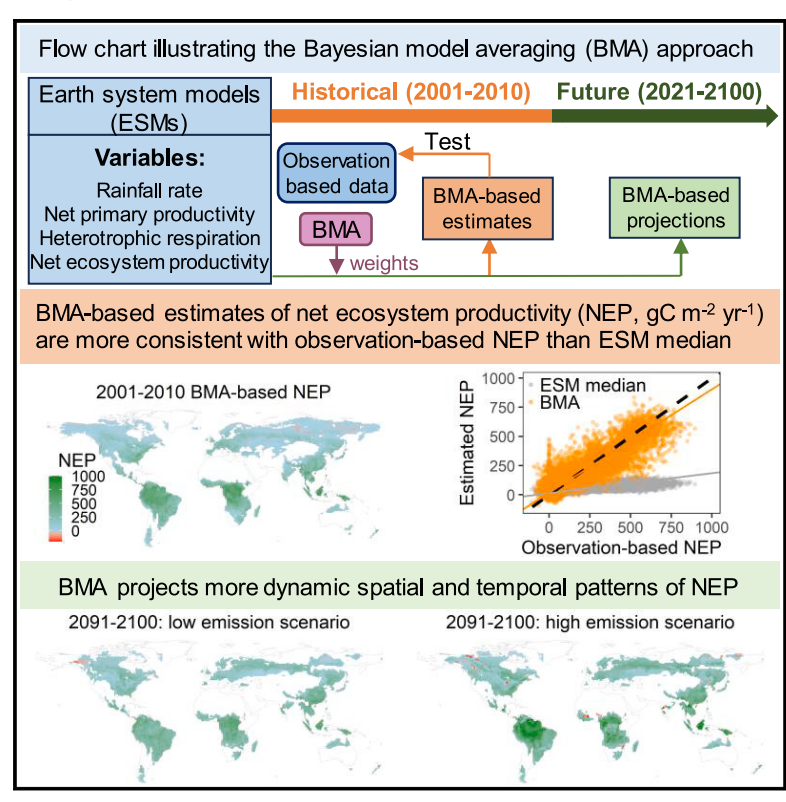
One Earth

Widespread temporal and spatial variability in net ecosystem productivity under climate change

Graphical abstract



Highlights

- Current model estimates of ecosystem carbon fluxes are relatively uncertain
- Bayesian model averaging (BMA) can constrain global carbon flux estimates
- BMA projects an unexpected higher variability of net ecosystem productivity (NEP)
- The NEP of Amazon forests will undergo significant changes under climate change

Authors

Heng Huang, Ignacio Rodriguez-Iturbe, Salvatore Calabrese

Correspondence

huangh557@mail.sysu.edu.cn (H.H.), salvatore.calabrese@ag.tamu.edu (S.C.)

In brief

Accurate projections of ecosystem carbon dynamics are important for enhancing global carbon storage and mitigating climate change. However, current estimation of ecosystem carbon balance by Earth system models remains highly uncertain. By merging new data and models, we reveal higher spatial and temporal variability of net ecosystem productivity than current model simulations. The net ecosystem productivity of Amazon forests, for example, may exhibit opposite trends under different climate scenarios. These improved estimates enable effective actions to protect ecosystem carbon storage.



Please cite this article in press as: Huang et al., Widespread temporal and spatial variability in net ecosystem productivity under climate change, One Earth (2024), https://doi.org/10.1016/j.oneear.2024.01.008

One Earth



Article

Widespread temporal and spatial variability in net ecosystem productivity under climate change

Heng Huang, 1,2,5,* Ignacio Rodriguez-Iturbe, 1,3,4 and Salvatore Calabrese 1,*

- ¹Department of Biological and Agricultural Engineering, Texas A&M University, College Station, TX 77843-2117, USA
- 2School of Ecology, Shenzhen Campus of Sun Yat-sen University, Shenzhen, Guangdong 518107, China
- ³Department of Ocean Engineering, Texas A&M University, College Station, TX 77843-3136, USA
- ⁴Department of Civil and Environmental Engineering, Texas A&M University, College Station, TX 77843-3136, USA
- *Correspondence: huangh557@mail.sysu.edu.cn (H.H.), salvatore.calabrese@ag.tamu.edu (S.C.) https://doi.org/10.1016/j.oneear.2024.01.008

SCIENCE FOR SOCIETY Climate change, due primarily to increasing carbon dioxide concentrations in the atmosphere, is posing a significant threat to natural and managed ecosystems. Particularly responsive to changing climate is the carbon balance: how much carbon an ecosystem absorbs and sequesters versus how much carbon it releases into the atmosphere. Climate mitigation plans reliant on ecosystems for carbon sequestration thus require accurate information on how climate change will impact their carbon balance. In this study, we built improved predictions showing that under climate change, ecosystem carbon balance is highly variable both in space and through time. Importantly, the impact on Amazon forests is sensitive to the level of warming, with carbon sequestration decreasing under low levels of warming while increasing under higher levels. Better carbon balance predictions will help inform which ecosystems will continue to absorb human emissions of carbon and where to focus climate mitigation efforts.

SUMMARY

The balance between net carbon assimilation by plants and carbon losses through heterotrophic respiration plays an important role in regulating the terrestrial carbon balance and the Earth's climate. The current high uncertainty in the magnitude of these carbon fluxes in Earth system models (ESMs), however, limits our ability to project the dynamics of net ecosystem productivity (NEP), which primarily determines to what extent ecosystems can store carbon. Here, we apply a data-model fusion approach to constrain global carbon flux estimates from ESMs. The analysis reveals that the spatial and temporal variability of NEP may be higher than currently expected from ESM simulations. Particularly, the NEP of Amazon forests is projected to decline considerably by the end of the century under SSP126 but will likely increase under higher emission scenarios due to the CO2 fertilization effect, highlighting the need for effective actions to maintain their C storage capacity under climate change.

INTRODUCTION

Understanding the dynamics of terrestrial ecosystem carbon (C) storage is crucial for implementing effective environmental policy and management strategies to enhance terrestrial C sequestration for climate change mitigation. Whether and to what extent an ecosystem can store C is primarily determined by the relative magnitude of two opposing ecosystem C fluxes, i.e., the vegetation net primary productivity (NPP) and heterotrophic respiration (R_h), whose difference is referred to as the net ecosystem productivity (NEP). The balance among these two fluxes as well as C emissions from disturbances such as fire and land use change control the terrestrial C pool, whose alteration can further influence the Earth's climate system through the climate-C cycle feedback.²⁻⁴ Unfortunately, accurate estimations of NPP, R_h , and NEP remain a challenge.

Recent environmental changes, including atmospheric CO2 rise, shifts in rainfall regime, land use change, and nitrogen deposition,⁵ have been driving a widespread greening of the world over the last several decades. 6-8 This worldwide greening is associated with an overall increase in NPP, which has the potential to enhance soil C storage and mitigate climate change. However, both empirical and modeling evidence also suggests an increasing trend of R_h globally, ^{9,10} likely due to increased substrate availability and/or enhanced soil organic C (SOC) mineralization under climate change (e.g., warming and changes in soil





moisture regime). Although recent work revealed the potential negative effect of future climate warming on Northern Hemisphere summer vegetation productivity, 11 the net impact of changes in NPP and R_h on ecosystem C storage remains relatively uncertain, as evidenced by the contradictory results from Earth system models (ESMs) and field experiments. 3,10,12 The recent IPCC Sixth Assessment Report (AR6) in fact reaffirms the highly uncertain future of the global land C sink, despite a reduction in the inter-model variability from the Coupled Model Intercomparison Project phase 5 (CMIP5) to CMIP6. 13 The significant uncertainty in C fluxes projections from ESMs may arise from imperfect model formulation and parameterization as well as from inaccurate representation of external variables influencing the terrestrial C dynamics. 14-16

As a result of these uncertainties, it remains unclear whether and to what extent the C balance of different ecosystems will be impacted by climate change.¹⁷ For example, forests are generally considered as a major C sink. 17-19 Recent evidence, however, suggests that tropical forests might act-locally-as a C source,²⁰ a fact that is not captured by ESMs. The ongoing intensification of environmental change such as land use change, drought, and fire disturbance may further reduce the C storage potential in tropical forests^{21,22} as well as in other ecosystems.¹⁷ Constraining the temporal and spatial dynamics of NPP, R_h, and NEP can significantly improve our capability to accurately project the impact of climate change on various ecosystems and enable a more efficient planning of land management strategies aimed at reducing C emissions and mitigating climate change.

The arithmetic multi-model averaging has been traditionally adopted in climate studies and IPCC reports to analyze climate model projections.²³ This approach is a form of "model democracy," whereby each model is given equal importance regardless of its performance. This, however, often leads to large differences between model estimates and observations,²⁴ making it clear that improved approaches to analyze ESMs are needed.²⁵ The recent emergence of data-driven global datasets of C fluxes offers new opportunities to adopt statistical approaches for data-model fusion to post-process the results of ESMs and obtain projections that are more consistent with observations. One such approach is Bayesian model averaging (BMA), 26 which leverages observations to compute a weighted average among different candidate models, with each model assigned a different weight depending on their performance in predicting a given variable under certain constraints. BMA has been applied to improve the estimates of hydrological processes such as rainfall and runoff.^{27,28} while whether and to what extent BMA can constrain global estimates of C fluxes remains largely unexplored. Given the large spread in ecosystem C flux simulations among ESMs, BMA provides an opportunity to improve the predictive accuracy of future land C dynamics under global change.

Here, we apply a land cover-specific BMA (LC-BMA) approach (see diagram in Figure S1), which averages CMIP6 ESMs²⁹ based on their performance in capturing a C flux (NPP, R_h, or NEP) within each land cover type. Taking advantage of the fact that ESMs, due to their different structures and parameterizations, may perform better in some land cover types and worse in others, BMA assigns for each land cover type a higher weight to better performing models, allowing us to obtain estimates that are overall more consistent with observations. We find that BMA-based historical estimates of ecosystem C fluxes are overall more consistent with global observation-based datasets than ESM ensemble estimates. BMA estimates also reveal higher variations in the spatial and temporal patterns of NEP. For instance, the NEP of Amazon forests may exhibit opposite trends under low and high carbon emission scenarios. Improving carbon balance projections by combining global datasets with ESMs (here through BMA) is crucial to support targeted environmental policy and management strategies to protect the C storage of climate-sensitive ecosystems.

RESULTS

Methods summary

We first test the performance of CMIP6 multi-model ensemble versus BMA estimates in capturing the observation-based C flux data during the historical period 2001-2010. We then apply BMA to CMIP6 models to project the future NEP from 2021 to 2100 under low (SSP126), medium (SSP370), and high (SSP585) emission scenarios by the end of the 21st century. We also analyze trends in NPP and R_h-the latter helped by a recently developed probabilistic soil microbial model that predicts long-term R_h from NPP and rainfall³⁰ (referred to as PMM hereafter) — to explore the major driving mechanisms (i.e., rainfall and/or NPP) of long-term NEP dynamics. The analysis includes 12 CMIP6 models (see Table S1 for details) with available rainfall, NPP, and R_h data for both historical and future scenarios (SSP126, SSP370, and SSP585, respectively).

Constraining global C flux estimates among ESMs via BMA

We begin by exploring the coefficient of variation (CV) of important drivers of NEP dynamics, namely rainfall (as a key input in PMM), NPP, and R_h, computed among the CMIP6 ESMs estimates during the historical 2001-2010 period. The analysis illustrates the relatively high variation in global rainfall, NPP, and R_h estimates among different ESMs (Figures 1A-1C and 1E). Specifically, NPP and R_h estimates are the most uncertain, with a higher intermodal variability in northern Canada, Western Asia, and Eastern Europe than other regions. Recently developed data-driven datasets (i.e., the CRU TS rainfall dataset, 31 the vegetation gross primary productivity [GPP] dataset based on an improved light use efficiency theory, 32 the CARDAMOM vegetation CUE dataset, 33 the R_h dataset by upscaling empirical observations from the Global Soil Respiration Database using random forest,34 and the FLUXCOM NEP database35) can be leveraged to improve these estimates. To constrain the uncertainty in historical rainfall, NPP, and R_h estimates from ESMs, we first divide the global data based on 11 land cover types and apply BMA for each land cover type (see experimental procedures and Figure S1). The results show that BMA-based rainfall and NPP estimates are overall more consistent with global data-driven databases (slope = 0.88 and 0.94, rootmean-square error [RMSE] = 0.09 and 114.1, both p < 0.001, respectively) than the CMIP6 ensemble median estimates (slope = 0.96 and 0.84, RMSE = 0.13 and 182.9, both p < 0.001, respectively), especially for high rainfall and NPP values (Figures 1B and 1D). Similarly, the BMA-based R_h



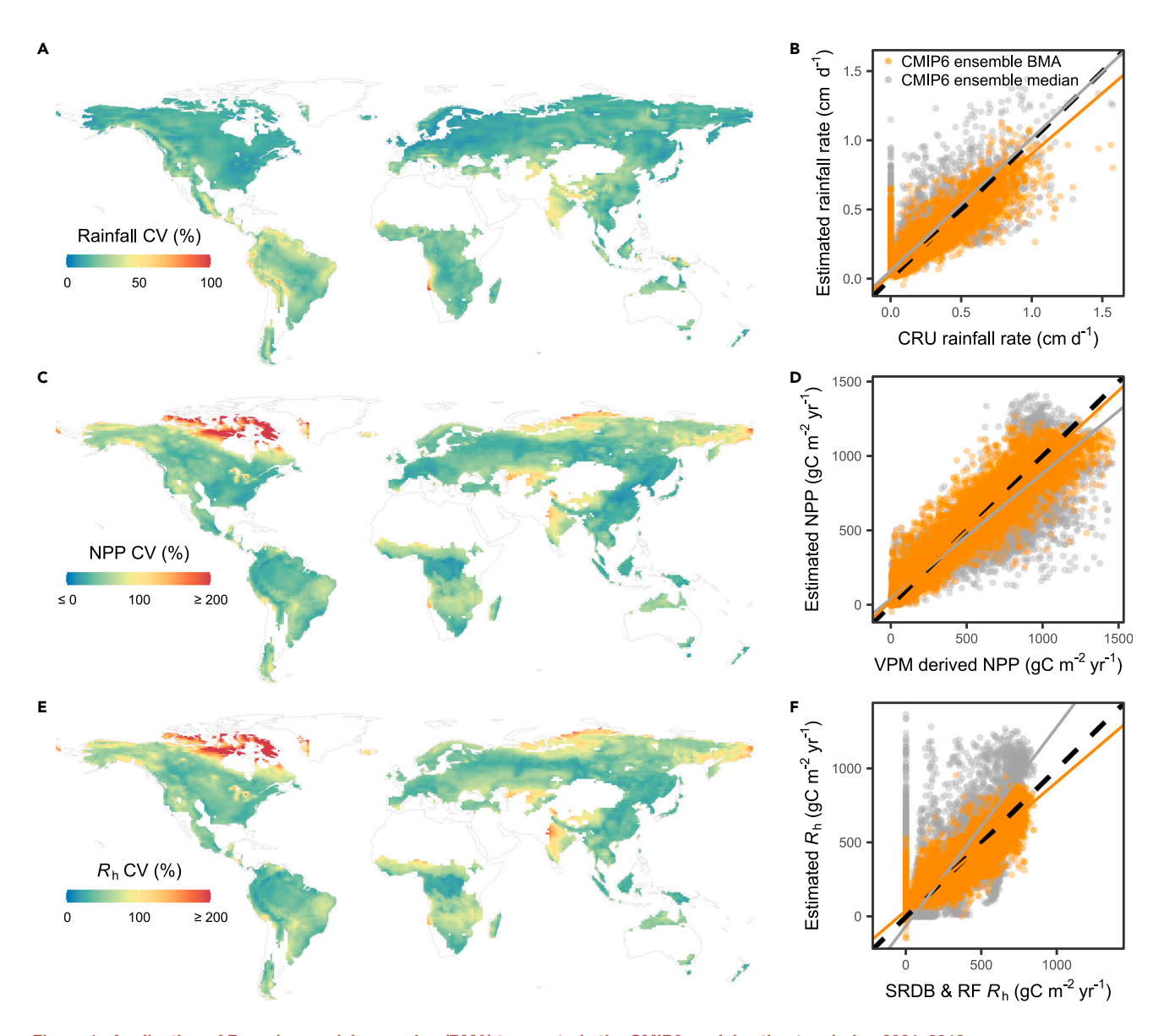


Figure 1. Application of Bayesian model averaging (BMA) to constrain the CMIP6 model estimates during 2001-2010

- (A) The global coefficient of variation (CV, %) of daily rainfall rate (cm day⁻¹) across 12 CMIP6 models.
- (B) Comparison of the performance of the CMIP6 ensemble BMA versus the CMIP6 ensemble median in estimating CRU rainfall data.
- (C) The global CV of annual vegetation net primary productivity (NPP, gC m⁻² yr⁻¹) across 12 CMIP6 models.
- (D) Comparison of the performance of the CMIP6 ensemble BMA versus the CMIP6 ensemble median in estimating VPM-derived NPP.
- (E) The global CV of annual heterotrophic respiration (R_h , gC m $^{-2}$ yr $^{-1}$) across 12 CMIP6 models.
- (F) Comparison of the performance of the CMIP6 ensemble BMA versus the CMIP6 ensemble median in estimating data-driven R_h. The black 1:1 line (dash) and the standardized major axis (SMA) regression lines (solid) are shown. The bare land was excluded from the analyses due to the high uncertainty in climate model output in this region.

estimates are more consistent with the global data-driven R_h dataset (slope = 0.87, RMSE = 94.8, p < 0.001) than the CMIP6 ensemble median estimates (slope = 1.35, RMSE = 201.2, p < 0.001) (Figure 1F), suggesting that BMA can be used as a robust approach to constrain the global estimates of rainfall, NPP, and R_h from ESMs.

We then apply BMA to directly constrain global NEP estimates from ESMs during 2001-2010. Both the observation-based FLUXCOM NEP (standard deviation SD = $193.5 \text{ gC m}^{-2} \text{ yr}^{-1}$) and BMA-based NEP (SD = 171.5) show a significantly higher degree of spatial variation than the CMIP6 ensemble median (SD = 33.3) during the historical period 2001-2010, with prominently higher NEP estimates in the eastern United States, South America, Central and Eastern Africa, and Southeastern Asia (Figures 2A-2C). The CMIP6 ensemble median NEP ranges from -4.3 to 187.2 gC m⁻² yr⁻¹ (global mean = 49.0), while the BMA-based NEP ranges from -91.8 to 832.6 gC m⁻² yr⁻¹ (global mean = 208.6) (Table 1).

Overall, the better performance following a BMA approach can be seen in Figure 2D, where BMA-based NEP estimates are



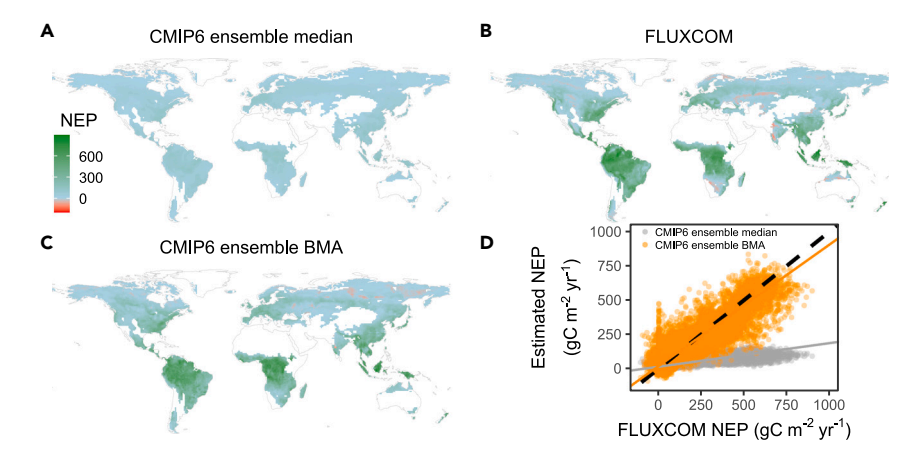


Figure 2. The high uncertainty in net ecosystem productivity (NEP) estimates by CMIP6 models

(A-C) The estimated global 10-year average NEP (gC $\,\mathrm{m}^{-2}\,\,\mathrm{yr}^{-1}$) during 2001-2010 by the CMIP6 ensemble median, FLUXCOM, and the CMIP6 ensemble BMA, respectively.

(D) Comparison of the performance of the CMIP6 ensemble BMA versus the CMIP6 ensemble median in estimating FLUXCOM NEP. The black 1:1 line (dash) and the standardized major axis (SMA) regression lines (solid) are shown. The bare land was excluded from the analyses due to the high uncertainty in climate model output in this region.

more positively correlated with FLUXCOM NEP across the globe (slope = 0.89, RMSE = 89.1, p < 0.001) than the CMIP6 ensemble median (slope = 0.17, RMSE = 208.4, p < 0.001). Figure 2D also reveals that the CMIP6 ensemble median estimates a relatively neutral NEP balance, regardless of the specific land cover type or geographic location. In addition, we also test the performance of each of the 12 ESMs and find that despite some variations across different ESMs, in general all models substantially underestimate the observation-based NEP (Figure S2).

Higher variability of NEP than currently projected

We then compare projections of global 10-year average annual NEP by BMA and the CMIP6 ensemble median from 2021-2030 to 2091-2100 under SSP126, SSP370, and SSP585. The CMIP6 ensemble median projections show minor changes in NEP by the end of the century, with consistently positive low values of NEP across the globe (Figure S3 and Table 1). By contrast, BMA projects a more pronounced spatial and temporal variability of NEP (Figure 3). Specifically, BMA projects a pronounced increase in NEP in some parts of North America, Europe, and Northern and Eastern Asia under all scenarios with a higher magnitude under SSP370 and SSP585. At the same time, BMA projects a decreasing trend in NEP in some parts of North and South America and Central Africa. Interestingly, BMA projects a considerable decline in NEP in Amazon forests by the end of the century under SSP126, but it projects a significant increase in NEP under higher emission scenarios (SSP370 and SSP585). Overall, BMA-based estimates show an increase of 44.1, 101.2, and 129.5 gC m⁻² yr⁻¹ in the mean NEP across the 11 land cover types under SSP126, SSP370, and SSP585, respectively, compared to a projected increase of 4.5, 35.4, and 51.5 gC $\,\mathrm{m^{-2}\,yr^{-1}}$ by the CMIP6 ensemble median (Table 1).

The major causes of future NEP changes

BMA also reveals different future patterns of NPP and $R_{\rm h}$ (Figures S4 and S5) from those expected based on the CMIP6 ensemble median (Figures S6 and S7). Specifically, the latter projects a more pronounced increasing trend in both NPP and $R_{\rm h}$ across most of the globe under SSP370 compared to SSP126 (Figures S6 and S7), with the tropics showing a greater increase in both NPP and $R_{\rm h}$ than other regions under all scenarios. In contrast, BMA projects a significant decline in NPP in

some tropical regions such as part of South America and Central and Eastern Africa under all scenarios (Figure S4). In addition, BMA projects a pronounced increase in R_h in many polar regions and a detectable decrease in part of South America and Southeastern Asia especially under SSP370 and SSP585 (Figure S5), which, according to PMM (used to link trends in R_h to changes in NPP and rainfall), results primarily from the same directional changes in NPP (Figure S4) and a projected decrease in rainfall rate in South America and Southeastern Asia (Figure S8). The BMA-projected increase in NEP in North America, Eastern Europe, and Eastern Asia is likely driven by the greater increase in NPP than R_h in these regions especially under SSP370 and SSP585 (Figures S4 and S5). In particular, BMA projects a decrease in NEP in Amazon forests by the end of the century under SSP126, which may be attributed to the greater increase in Rh than NPP in these regions. However, BMA projects an increase in NEP in Amazon forests by the end of the century under SSP370 and SSP585. This is mainly a result of the enhanced NPP under higher emission scenarios, given the less significant changes in R_h due to the future decline in rainfall (Figure S8).

DISCUSSION

Our findings reveal that the historical global estimates of NPP and R_h are highly uncertain across CMIP6 ESMs, as evident from the high CV in CMIP6 ensemble estimates across the globe (Figures 1C and 1E). Given that NEP is the difference between NPP and R_h , uncertainties in NPP and R_h compound in NEP. Recent data-driven global datasets contain important information about ecosystem dynamics that can be leveraged to constrain CMIP6 predictions. The LC-BMA approach significantly improves the agreement between global NEP estimates and observations (Figure 2). The CMIP6 ensemble median NEP estimates are overall positive but low, with relatively uniform spatial patterns across the globe during 2001-2010. This appears unlikely, as the observation-based FLUXCOM NEP database suggests a high spatial variation across the globe. The NEP estimates from each single ESM as well as the ensemble median in fact show a weak correlation with FLUXCOM NEP (Figures 2D and S2), underlining the current high uncertainty in estimating the terrestrial C balance. In contrast, the BMA-based NEP shows a good agreement with FLUXCOM NEP, providing



Table 1. Summary of the terrestrial 10-year average NEP (gC m⁻² yr⁻¹) estimated by the CMIP6 ensemble median and BMA during the historical and future periods

| Latitudinal zone | Method | 2001–2010 | SSP | 2021–2030 | 2051–2060 | 2091–2100 |
|-------------------------|--------------|----------------------|-----|------------------------|------------------------|------------------------|
| Tropical (0°-23.5°) | CMIP6 median | 68.8 (0.4, 187.2) | 126 | 82.1 (4.8, 214.2) | 82.7 (0.3, 232.2) | 61.7 (-1.2, 197.5) |
| | | | 370 | 82.7 (0.6, 216.6) | 96.6 (2.3, 261.1) | 103.2 (-51.7, 298.3) |
| | | | 585 | 79.0 (-1.4, 250.8) | 109.4 (1.4, 337.1) | 128.4 (-1.6, 506.0) |
| | ВМА | 367.8 (-91.8, 832.6) | 126 | 365.9 (-166.0, 861.9) | 379.7 (-120.6, 816.2) | 336.1 (-138.0, 689.5) |
| | | | 370 | 379.6 (-124.2, 944.2) | 416.4 (-206.0, 1129.0) | 418.1 (-236.2, 1370.3) |
| | | | 585 | 352.3 (-173.8, 1005.9) | 438.8 (-359.4, 1155.5) | 473.0 (-254.3, 1321.1) |
| Temperate (23.5°–66.5°) | CMIP6 median | 39.7 (-4.3, 136.8) | 126 | 52.1 (-4.1, 206.0) | 60.0 (0, 206.0) | 48.1 (-1.4, 194.6) |
| | | | 370 | 47.1 (-0.6, 174.2) | 63.6 (-0.7, 238.2) | 72.4 (-1.6, 283.4) |
| | | | 585 | 48.3 (-45.7, 202.9) | 66.9 (0, 341.4) | 81.9 (-0.4, 274.3) |
| | BMA | 120.0 (-72.8, 631.5) | 126 | 186.9 (-67.3, 644.1) | 212.5 (-73.6, 669.4) | 187.0 (-148.8, 591.5) |
| | | | 370 | 166.4 (-153.2, 748.3) | 205.3 (-237.5, 679.3) | 233.1 (-231.6, 810.2) |
| | | | 585 | 167.7 (-576.5, 672.5) | 210.4 (-223.3, 744.2) | 241.3 (-223.3, 791.5) |
| Polar (66.5°-90°) | CMIP6 median | 4.3 (-4.3, 23.4) | 126 | 2.5 (-1.0, 19.0) | 3.3 (-1.9, 19.5) | 3.4 (-2.2, 22.8) |
| | | | 370 | 1.7 (-1.3, 26.8) | 4.1 (-3.1, 25.6) | 3.5 (-3.6, 43.7) |
| | | | 585 | 2.6 (-1.8, 58.6) | 4.1 (-1.7, 63.6) | 4.5 (-4.6, 90.2) |
| | ВМА | 9.8 (-44.2, 110.5) | 126 | 47.5 (-33.9, 152.6) | 56.3 (-33.0, 129.2) | 56.5 (-43.0, 136.7) |
| | | | 370 | 35.4 (-40.9, 137.0) | 53.5 (-41.7, 165.6) | 49.8 (-292.4, 207.8) |
| | | | 585 | 40.5 (-38.6, 153.5) | 50.9 (-50.1, 174.2) | 42.5 (-300.3, 191.2) |
| Global | CMIP6 median | 49.0 (-4.3, 187.2) | 126 | 64.9 (-4.1, 214.2) | 69.4 (-1.9, 232.2) | 53.5 (-2.2, 197.5) |
| | | | 370 | 61.6 (-1.3, 216.6) | 76.7 (-3.1, 261.1) | 84.4 (-51.7, 298.3) |
| | | | 585 | 60.7 (-45.7, 250.8) | 84.1 (-1.7, 341.4) | 100.5 (-4.6, 506.0) |
| | BMA | 208.6 (-91.8, 832.6) | 126 | 266.1 (-166.0, 861.9) | 286.0 (-120.6, 816.2) | 252.7 (-148.8, 689.5) |
| | | | 370 | 256.5 (-153.2, 944.2) | 294.0 (-237.5, 1129.0) | 309.8 (-292.4, 1370.3) |
| | | | 585 | 245.5 (-576.5, 1005.9) | 306.6 (-359.4, 1155.5) | 338.1 (-300.3, 1321.1) |
| | | | | | | |

The area-weighted mean as well as the minimum and maximum values are shown. The grid cells dominated by the 11 land cover types (i.e., tropical evergreen trees, tropical deciduous trees, extra-tropical evergreen trees, extra-tropical deciduous trees, shrubs, C3 grass, C4 grass, C3 pasture, C4 pasture, C3 crops, and C4 crops) were included for the analysis. The bare land was excluded from the analyses due to the high uncertainty in climate model output in this region.

support to the idea that "model democracy" may not yield realistic estimates.²⁴ We note that in this study, we did not specifically account for internal model variability since only a few CMIP6 models provide multiple ensemble members for both historical and future periods. Recent work has shown that internal model variability might also contribute to model uncertainty in climate estimates and projections. 36,37 This highlights the need for producing multiple ensemble members for each model in the upcoming CMIP7 simulations, which will enable critical assessments of the contributions of internal model variability to model uncertainty.

Although recent evidence suggests a potential shift in the summer GPP-temperature relationship from positive to negative in the Northern Hemisphere under future climate warming,11 the future NEP dynamics under climate change remain highly uncertain, as demonstrated by the disagreement between ESMs and field experiments. 3,10,12 The BMA analysis suggests a considerably higher spatial and temporal variability of NEP than ESM projections especially under higher emission scenarios, highlighting the critical need for improved simulations of land C dynamics in ESMs. Moreover, BMA projections suggest that some regions such as part of North and South America and Africa will experience a significant decline in NEP due to the decrease in NPP or the greater increase in R_h than NPP (Figures 3, S4, and S5), therefore potentially reducing the C storage capacity of these ecosystems. Notably, the NEP in Amazon forests is projected to decline considerably by the end of the century under SSP126. This is consistent with previous work suggesting a long-term decline in tropical forest carbon sink over the past several decades^{38,39} which will likely continue in the future. 40 However, BMA analysis also suggests that the NEP in Amazon forests will likely increase under SSP370 and SSP585, owing to the enhanced NPP induced by the CO₂ fertilization effect.⁶⁻⁸ In addition, the projected decrease in rainfall in Amazon forests under higher emission scenarios limits the magnitude of the changes in R_h according to PMM, therefore further enhancing the NEP in Amazon forests.

Although BMA shows a greater capacity to constrain the historical C flux estimates among ESMs, there might exist uncertainty in transferring the land cover-specific BMA weights from the historical period to the future climate scenarios. For example, the ongoing environmental changes and their interactions may confound their current impacts on climate and C dynamics and therefore affect the consistency of the model's performance in historical and future simulations. These aspects are still highly



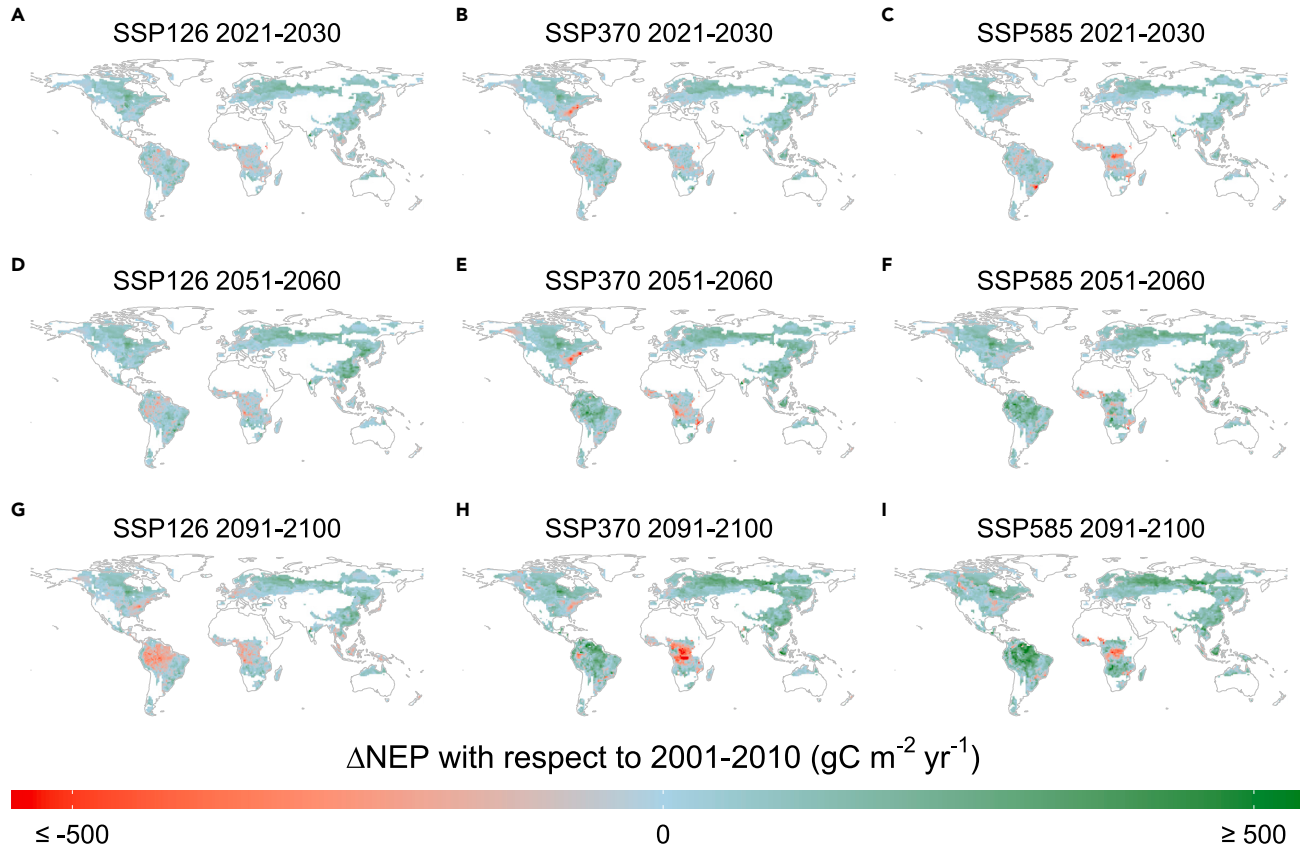


Figure 3. Global projections of 10-year average annual NEP (gC m⁻² yr⁻¹) by CMIP6 ensemble BMA during 2021-2100

(A, D, and G) Projections under SSP126.

(B, E, and H) Projections under SSP370.

(C, F, and I) Projections under SSP585. The bare land was excluded from the analyses due to the high uncertainty in climate model output in this region.

unpredictable and need to be better represented in ESMs, which will consequently improve the accuracy of BMA projections. Yet, BMA weights assigned based on historical data still remain our best guess for future projections. In addition, even though we have accounted for the future land cover change in our BMA analysis, we note that other environmental changes such as drought, fire disturbance, and land degradation will also jointly alter global C balance. 17,21 For example, drought-induced tree mortality may turn ecosystems from C sinks to sources. 41,42 Moreover, future land cover change is highly uncertain⁴³ and may further alter the dynamics of NEP, although it should have limited effects on our results because we focus on relatively long-term NEP dynamics at the regional scale. Nevertheless, these factors should be considered for accurate assessment of net ecosystem C balance. The development of effective environmental policy and management, such as the adoption of nature-based solutions or land-based CO₂ removal (e.g., enhanced weathering), 45,46 may be required for regions that show strong NEP dynamics under climate change to achieve ecosystem sustainability and C neutrality. 1 Restoration efforts aiming to increase vegetation productivity, such as afforestation, reforestation, and sustainable forest management, might be a potentially important approach to enhance ecosystem C storage, 47,48 although increased C inputs might also accelerate soil C decomposition. 49

While fusion of model and global data provides a valuable approach to post-process ESM projections, we would like to note that the accuracy of the fused product necessarily depends on the quality of the global data input. The FLUXCOM NEP estimates, which are based on the upscaling of FLUXNET eddy covariance data using machine learning algorithms, may carry some biases from the upscaling algorithm or the data input.4 In fact, scaling up from site-level NEP measurements to regional-scale patterns remains a challenge, as it introduces a variety of uncertainties related to the inhomogeneity in rainfall regimes and vegetation and soil types within each grid cell. 4,17 Yet, BMA remains a valuable and simple approach to constrain global estimates of C fluxes, and -as observationbased databases improve—the accuracy of the fused product will also improve, especially if BMA can be based on simultaneous observations of multiple variables (and not NEP only). In addition to BMA, other statistical weighting approaches that have been developed and applied for climate projections^{50,51} could also be leveraged to improve the estimates of terrestrial C dynamics and merit further investigation.

Lastly, our analysis—also helped by PMM³⁰ (see Note S1) suggests that the current high uncertainty in both NPP and R_h estimates from ESMs may be one of the major causes leading to uncertain NEP estimation (Figures 1, 2, S9, and S10). In fact,



R_h has already been regarded as one of the most poorly constrained ecosystem C fluxes,52 and many ESMs still model Rh based on simplified kinetics of soil C dynamics, which result in a nearly proportional relationship with NPP (Figure S11A). This is unlikely, as evidenced by site-level observations and datadriven global datasets (Figures S11B and S11C). Efforts are thus required to reduce the uncertainty in the key biogeochemical processes underlying both NPP and R_h in ESMs. Promising approaches are being developed to improve vegetation models based on optimality principles⁵³ and to expand soil C models to explicitly include microbial processes.⁵⁴⁻⁵⁸ These novel model structures and parameterizations 14-16 are being successful in capturing the response of biological systems to environmental changes and, if combined with the utilization of global empirical datasets, may offer an opportunity to significantly enhance the performance of ESMs in predicting the terrestrial C balance.

EXPERIMENTAL PROCEDURES

Resource availability

Lead contact

Further information and requests for resources should be directed to Heng Huang (huangh557@mail.sysu.edu.cn).

Materials availability

This study did not generate new unique materials.

Data and code availability

The CMIP6 rainfall and C flux datasets are available at https://esgf-node.llnl.gov/ projects/cmip6/. The CRU temperature and rainfall datasets are available at https://crudata.uea.ac.uk/cru/data/hrg/. The FLUXCOM NEP database is available at https://www.fluxcom.org/. The VPM GPP dataset is available at https:// doi.org/10.6084/m9.figshare.c.3789814. The CARDAMOM vegetation CUE dataset is available at https://datashare.ed.ac.uk/handle/10283/875. The datadriven global heterotrophic respiration dataset is available at https://figshare. com/articles/dataset/global_SHR_datasets_zip/11340770. The R code developed in this study can be found at https://osf.io/x5usc/?view_only=82c861cf2d 5a4d02a8bc9145855fcab4.

CMIP6 multi-model ensemble

To limit biases from individual model formulations, we used the multi-model ensemble of CMIP6 to compare rainfall and C flux estimates between BMA and ESMs. We selected 12 CMIP6 models (see Table S1 for details) that provide available monthly rainfall, NPP, $R_{\rm h}$, and NEP data for both historical and three future scenarios (i.e., shared socioeconomic pathways SSP126, SSP370, and SSP585, representing low, medium, and high radiative forcing by the end of the 21st century, respectively). For all ESMs, the ensemble member "r1i1p1f1" was chosen. Prior to analyses, all CMIP6 models were resampled to the same spatial resolution ($1^{\circ} \times 1^{\circ}$) using the bilinear interpolation approach. We focused on the 10-year average (i.e., 2001-2010 for the historical period, and from 2021-2030 to 2051-2060 and 2091-2100 for future scenarios) to smooth out time-series fluctuations and to yield more steady and robust results.

Bayesian model averaging for historical rainfall, NPP, R_b, and NEP

We applied the BMA²⁶ approach using the bicreg function from the R package BMA⁵⁹ to constrain the estimates of rainfall, NPP, R_h, and NEP among 12 ESMs during the 2001-2010 period. BMA is a postprocessing approach that merges multi-model ensemble into a fused version based on the following equation:

$$p(y|f_1,...,f_K) = \sum_{k=1}^K w_k g_k(y|f_k),$$
 [Equation 1]

where y represents the quantity to be forecasted, f_k represents the forecasts from each of the K different models, which are linear functions of different combinations of ESMs, i.e., $f_k = \sum_{i=1}^{12} (a + b_i \text{ESM}_i)$, w_k is the posterior probability of forecast k being the best one and indicates each model's predictive capacity in the training period, and $g_k(y|f_k)$ represents the conditional probability density function of y conditional on f_k , given that f_k is the best model. The parameters a and b_i are estimated through linear regression analysis of empirical observations versus ESM estimates. The use of parameters a and b_i can be considered as a simple statistical approach to correct the bias in model forecasts. The BMA predictive mean (Y) can be calculated as follows:

$$Y = \sum_{k=1}^{K} w_k f_k.$$
 [Equation 2]

Detailed descriptions of BMA can be found in Raftery et al.^{26,59}

The data-driven global datasets used in the BMA analyses include the CRU TS rainfall dataset,31 the GPP dataset based on an improved light use efficiency theory, 32 the CARDAMOM vegetation CUE dataset, 33 the R_h dataset by upscaling empirical observations from the Global Soil Respiration Database using a random forest ensemble machine learning algorithm,³⁴ and the FLUXCOM NEP database created by upscaling the eddy covariance C flux observations using multiple machine learning methods (random forest, multivariate regression splines, and artificial neural network). 35 The ensemble median of $\ensuremath{\textit{R}}_{\text{h}}$ and NEP datasets based on different machine learning approaches and/or different input datasets was chosen for our analysis. We applied BMA analysis independently to obtain BMA-based estimates of rainfall, NPP, $R_{\rm h}$, and NEP. The BMA analysis was conducted for each of the 11 land cover types (i.e., tropical evergreen trees, tropical deciduous trees, extra-tropical evergreen trees, extra-tropical deciduous trees, shrubs, C3 grass, C4 grass, C3 pasture, C4 pasture, C3 crops, and C4 crops) based on the land cover data from the model MPI-ESM1-2-LR, which was chosen because it provides a detailed land cover classification and also showed a good agreement with the observed vegetation distribution.60 We note that the land cover type "bare land" was excluded from the analyses due to the high uncertainty in climate model output in this region. The deciduous and "raingreen" (i.e., drought-deciduous) shrubs were merged into a larger classification (i.e., shrubs) due to the relatively limited number of grid cells for both land cover types. We calculated the mean fractional cover of each land cover type within each 1° x grid cell during 2001-2010. The land cover type with the maximum factional cover was used to represent the land cover type for each grid cell. We then conducted the standardized major axis regression (SMA) regression using the Imodel2 function from the R package Imodel2⁶¹ to examine the congruence between BMA-based estimates and data-driven gridded datasets for rainfall, NPP, R_h, and NEP, respectively.

Calibration of PMM based on global data-driven datasets

Given that ecosystem models, such as ESMs, can be computationally complex, simple models, or so-called emulators, may be more amenable to and efficient in model uncertainty analysis and calibration. 62,63 In this regard, we have recently developed a parsimonious probabilistic soil microbial model (PMM) to describe the temporal dynamics of R_h across different ecosystems worldwide as driven by dominant environmental factors.30 When resolved over long temporal scales, PMM suggests that the annual R_h (gC m⁻² yr⁻¹) is mainly controlled by rainfall characteristics and NPP, and it can be predicted from $R_h = C * R^{\alpha} * NPP^{\beta}$, where C is a constant, R is the mean rainfall rate over the studied time frame (cm day⁻¹), and α and β are exponents of R and NPP, respectively. As shown in Huang et al., 30 the model predictions were well supported by empirical observations from the FLUXNET 2015 database, demonstrating the robustness of PMM. The functional form based on power laws also allows upscaling from ecosystem to regional scale by adjusting the power-law exponents.

We refitted the parameters in PMM to increase model accuracy using the data-driven global R_h dataset,³⁴ since the original model parameters were estimated based on site-level data, and it is expected that scaling up from the site level to regional level involves additional uncertainties in input variables that need to be reduced through the calibration of PMM. Through nonlinear regression analysis using the nls function from the R package stats, we obtained the calibrated upscaled PMM, which is expressed as $R_h = 64.84 * R^{0.24} * NPP^{0.35}$. The SMA regression analysis was conducted, and the RMSE was also calculated to test the consistency between PMM estimates and global $R_{\rm h}$ dataset.

Please cite this article in press as: Huang et al., Widespread temporal and spatial variability in net ecosystem productivity under climate change, One Earth (2024), https://doi.org/10.1016/j.oneear.2024.01.008





We note that although temperature has been widely considered as an important factor influencing $R_{\rm h}^{64}$ we found that the effect of temperature on long-term $R_{\rm h}$ across the globe was relatively weak and has been primarily accounted for in PMM (see Note S2 and Figure S12).

Projecting the future global NPP, $R_{\rm h}$, and NEP patterns

We first tested the performance of BMA and PMM versus the CMIP6 multimodel ensemble median in estimating the FLUXCOM NEP (gC m $^{-2}$ yr $^{-1}$) during the 2001–2010 period. The PMM-based global NEP was estimated as the BMA-based NPP minus the PMM-based $R_{\rm h}$. The CMIP6 ensemble median NEP was calculated as the median of the NEP estimates from the selected 12 CMIP6 models. As mentioned above, we also calculated the BMA-based global NEP directly using the NEP estimates from 12 CMIP6 ESMs. SMA regression analysis was conducted to test the consistency between estimates from different approaches (BMA, PMM, and the CMIP6 ensemble median) and FLUXCOM NEP across the globe.

We then retrieved global data from 12 CMIP6 models to project the 10-year average rainfall, NPP, $R_{\rm h}$, and NEP during the 2021–2100 period. Data from SSP126, SSP370, and SSP585 were used to compare projections under different future emission scenarios. In order to constrain the uncertainty in CMIP6 model projections, we utilized the land cover-specific BMA weights for the 2001–2010 period to obtain BMA-based projections of 10-year average global rainfall, NPP, $R_{\rm h}$, and NEP during 2021–2100 and compared their performance with the CMIP6 ensemble median. To account for the land use and land cover change in the future, we retrieved the land cover projections during 2021–2100 from the model MPI-ESM1-2-LR and calculated the fractional cover of each land cover type for each 10-year period to determine the land cover type of each grid in the future.

SUPPLEMENTAL INFORMATION

Supplemental information can be found online at https://doi.org/10.1016/j.oneear.2024.01.008.

ACKNOWLEDGMENTS

This work was supported by the National Science Foundation (DEB-2213630), the USDA National Institute of Food and Agriculture (Hatch project 1023954), and the Department of Biological and Agricultural Engineering and AgriLife Research at Texas A&M University.

AUTHOR CONTRIBUTIONS

 $\mbox{H.H.},$ S.C., and I.R.-I. conceived the study; H.H. analyzed the data; H.H., S.C., and I.R.-I. wrote the paper.

DECLARATION OF INTERESTS

The authors declare no competing interests.

Received: February 21, 2023 Revised: November 13, 2023 Accepted: January 11, 2024 Published: February 2, 2024

REFERENCES

- Bossio, D.A., Cook-Patton, S.C., Ellis, P.W., Fargione, J., Sanderman, J., Smith, P., Wood, S., Zomer, R.J., Von Unger, M., Emmer, I.M., and Griscom, B.W. (2020). The role of soil carbon in natural climate solutions. Nat. Sustain. 3, 391–398.
- Davidson, E.A., and Janssens, I.A. (2006). Temperature sensitivity of soil carbon decomposition and feedbacks to climate change. Nature 440, 165–173.
- Todd-Brown, K.E.O., Randerson, J.T., Hopkins, F., Arora, V., Hajima, T., Jones, C., Shevliakova, E., Tjiputra, J., Volodin, E., Wu, T., et al. (2014). Changes in soil organic carbon storage predicted by Earth system models during the 21st century. Biogeosciences 11, 2341–2356.

- 4. Keenan, T.F., and Williams, C.A. (2018). The Terrestrial Carbon Sink. Annu. Rev. Environ. Resour. *43*, 219–243.
- Piao, S., Wang, X., Park, T., Chen, C., Lian, X., He, Y., Bjerke, J.W., Chen, A., Ciais, P., Tømmervik, H., et al. (2019). Characteristics, drivers and feedbacks of global greening. Nat. Rev. Earth Environ. 1, 14–27.
- Myneni, R.B., Keeling, C.D., Tucker, C.J., Asrar, G., and Nemani, R.R. (1997). Increased plant growth in the northern high latitudes from 1981 to 1991. Nature 386. 698–702.
- Nemani, R.R., Keeling, C.D., Hashimoto, H., Jolly, W.M., Piper, S.C., Tucker, C.J., Myneni, R.B., and Running, S.W. (2003). Climate-driven increases in global terrestrial net primary production from 1982 to 1999. Science 300, 1560–1563.
- Zhu, Z., Piao, S., Myneni, R.B., Huang, M., Zeng, Z., Canadell, J.G., Ciais, P., Sitch, S., Friedlingstein, P., Arneth, A., et al. (2016). Greening of the Earth and its drivers. Nat. Clim. Change 6, 791–795.
- Bond-Lamberty, B., Bailey, V.L., Chen, M., Gough, C.M., and Vargas, R. (2018). Globally rising soil heterotrophic respiration over recent decades. Nature 560, 80–83.
- Naidu, D.G.T., and Bagchi, S. (2021). Greening of the earth does not compensate for rising soil heterotrophic respiration under climate change. Global Change Biol. 27, 2029–2038.
- Zhang, Y., Piao, S., Sun, Y., Rogers, B.M., Li, X., Lian, X., Liu, Z., Chen, A., and Peñuelas, J. (2022). Future reversal of warming-enhanced vegetation productivity in the Northern Hemisphere. Nat. Clim. Change 12, 581–586.
- Wieder, W.R., Sulman, B.N., Hartman, M.D., Koven, C.D., and Bradford, M.A. (2019). Arctic soil governs whether climate change drives global losses or gains in soil carbon. Geophys. Res. Lett. 46, 14486–14495.
- V. Masson-Delmotte, P. Zhai, A. Pirani, S.L. Connors, C. Péan, S. Berger, N. Caud, Y. Chen, L. Goldfarb, and M.I. Gomis, et al., eds. (2021). IPCC, 2021: Climate Change 2021: The Physical Science Basis. Contribution of Working Group I to the Sixth Assessment Report of the Intergovernmental Panel on Climate Change (Cambridge University Press).
- Luo, Y., Ahlström, A., Allison, S.D., Batjes, N.H., Brovkin, V., Carvalhais, N., Chappell, A., Ciais, P., Davidson, E.A., Finzi, A., et al. (2016). Toward more realistic projections of soil carbon dynamics by Earth system models. Global Biogeochem. Cycles 30, 40–56.
- Bonan, G.B., and Doney, S.C. (2018). Climate, ecosystems, and planetary futures: The challenge to predict life in Earth system models. Science 359, eaam8328.
- Padrón, R.S., Gudmundsson, L., Liu, L., Humphrey, V., and Seneviratne, S.I. (2022). Drivers of intermodel uncertainty in land carbon sink projections. Biogeosciences 19, 5435–5448.
- Yang, Y., Shi, Y., Sun, W., Chang, J., Zhu, J., Chen, L., Wang, X., Guo, Y., Zhang, H., Yu, L., et al. (2022). Terrestrial carbon sinks in China and around the world and their contribution to carbon neutrality. Sci. China Life Sci. 65, 861–895.
- Pan, Y., Birdsey, R.A., Fang, J., Houghton, R., Kauppi, P.E., Kurz, W.A., Phillips, O.L., Shvidenko, A., Lewis, S.L., Canadell, J.G., et al. (2011). A large and persistent carbon sink in the world's forests. Science 333, 988–993.
- Tagesson, T., Schurgers, G., Horion, S., Ciais, P., Tian, F., Brandt, M., Ahlström, A., Wigneron, J.P., Ardö, J., Olin, S., et al. (2020). Recent divergence in the contributions of tropical and boreal forests to the terrestrial carbon sink. Nat. Ecol. Evol. 4, 202–209.
- Baccini, A., Walker, W., Carvalho, L., Farina, M., Sulla-Menashe, D., and Houghton, R.A. (2017). Tropical forests are a net carbon source based on aboveground measurements of gain and loss. Science 358, 230–234.
- 21. Qin, Y., Xiao, X., Wigneron, J.P., Ciais, P., Brandt, M., Fan, L., Li, X., Crowell, S., Wu, X., Doughty, R., et al. (2021). Carbon loss from forest degradation exceeds that from deforestation in the Brazilian Amazon. Nat. Clim. Change 11, 442–448.
- 22. Mitchard, E.T.A. (2018). The tropical forest carbon cycle and climate change. Nature 559, 527-534.

One Earth

Article



- 23. Eyring, V., Cox, P.M., Flato, G.M., Gleckler, P.J., Abramowitz, G., Caldwell, P., Collins, W.D., Gier, B.K., Hall, A.D., Hoffman, F.M., et al. (2019). Taking climate model evaluation to the next level. Nat. Clim. Change 9, 102-110.
- 24. Hausfather, Z., Marvel, K., Schmidt, G.A., Nielsen-Gammon, J.W., and Zelinka, M. (2022). Climate simulations: Recognize the "hot model" problem. Nature 605, 26-29,
- 25. Knutti, R. (2010). The end of model democracy? Clim. Change 102, 395-404.
- 26. Raftery, A.E., Gneiting, T., Balabdaoui, F., and Polakowski, M. (2005). Using Bayesian model averaging to calibrate forecast ensembles. Mon. Weather Rev. 133, 1155-1174.
- 27. Yang, H., Zhou, F., Piao, S., Huang, M., Chen, A., Ciais, P., Li, Y., Lian, X., Peng, S., and Zeng, Z. (2017). Regional patterns of future runoff changes from Earth system models constrained by observation. Geophys. Res. Lett. 44, 5540-5549.
- 28. Massoud, E.C., Lee, H., Gibson, P.B., Loikith, P., and Waliser, D.E. (2020). Bayesian model averaging of climate model projections constrained by precipitation observations over the contiguous United States. J. Hydrometeorol. 21, 2401-2418.
- 29. Eyring, V., Bony, S., Meehl, G.A., Senior, C.A., Stevens, B., Stouffer, R.J., and Taylor, K.E. (2016). Overview of the Coupled Model Intercomparison Project Phase 6 (CMIP6) experimental design and organization. Geosci. Model Dev. (GMD) 9, 1937-1958.
- 30. Huang, H., Calabrese, S., and Rodriguez-Iturbe, I. (2021). Variability of ecosystem carbon source from microbial respiration is controlled by rainfall dynamics. Proc. Natl. Acad. Sci. USA 118. e2115283118.
- 31. Harris, I., Osborn, T.J., Jones, P., and Lister, D. (2020). Version 4 of the CRU TS monthly high-resolution gridded multivariate climate dataset. Sci. Data 7, 109.
- 32. Zhang, Y., Xiao, X., Wu, X., Zhou, S., Zhang, G., Qin, Y., and Dong, J. (2017). A global moderate resolution dataset of gross primary production of vegetation for 2000-2016. Sci. Data 4, 170165.
- 33. Bloom, A.A., Exbrayat, J.F., Van Der Velde, I.R., Feng, L., and Williams, M. (2016). The decadal state of the terrestrial carbon cycle: Global retrievals of terrestrial carbon allocation, pools, and residence times. Proc. Natl. Acad. Sci. USA 113, 1285-1290.
- 34. Yao, Y., Ciais, P., Viovy, N., Li, W., Cresto-Aleina, F., Yang, H., Joetzjer, E., and Bond-Lamberty, B. (2021). A data-driven global soil heterotrophic respiration dataset and the drivers of its inter-annual variability. Global Biogeochem. Cycles 35. e2020GB006918.
- 35. Jung, M., Schwalm, C., Migliavacca, M., Walther, S., Camps-Valls, G., Koirala, S., Anthoni, P., Besnard, S., Bodesheim, P., Carvalhais, N., et al. (2020). Scaling carbon fluxes from eddy covariance sites to globe: synthesis and evaluation of the FLUXCOM approach. Biogeosciences 17. 1343-1365.
- 36. Lehner, F., Deser, C., Maher, N., Marotzke, J., Fischer, E.M., Brunner, L., Knutti, R., and Hawkins, E. (2020). Partitioning climate projection uncertainty with multiple large ensembles and CMIP5/6. Earth Syst. Dynam. 11, 491-508.
- 37. Tebaldi, C., Debeire, K., Eyring, V., Fischer, E., Fyfe, J., Friedlingstein, P., Knutti, R., Lowe, J., O'Neill, B., Sanderson, B., et al. (2021). Climate model projections from the Scenario Model Intercomparison Project (ScenarioMIP) of CMIP6. Earth Syst. Dynam. 12, 253-293.
- 38. Brienen, R.J.W., Phillips, O.L., Feldpausch, T.R., Gloor, E., Baker, T.R., Lloyd, J., Lopez-Gonzalez, G., Monteagudo-Mendoza, A., Malhi, Y., Lewis, S.L., et al. (2015). Long-term decline of the Amazon carbon sink. Nature 519, 344-348.
- 39. Koch, A., Hubau, W., and Lewis, S.L. (2021). Earth System Models are not capturing present-day tropical forest carbon dynamics. Earth's Future 9. e2020EF001874.
- 40. Hubau, W., Lewis, S.L., Phillips, O.L., Affum-Baffoe, K., Beeckman, H., Cuní-Sanchez, A., Daniels, A.K., Ewango, C.E.N., Fauset, S., Mukinzi,

- J.M., et al. (2020). Asynchronous carbon sink saturation in African and Amazonian tropical forests. Nature 579, 80-87.
- 41. Allen, C.D., Macalady, A.K., Chenchouni, H., Bachelet, D., McDowell, N., Vennetier, M., Kitzberger, T., Rigling, A., Breshears, D.D., Hogg, E.T., et al. (2010). A global overview of drought and heat-induced tree mortality reveals emerging climate change risks for forests. For. Ecol. Manage. 259, 660-684
- 42. Anderegg, W.R.L., Kane, J.M., and Anderegg, L.D.L. (2013). Consequences of widespread tree mortality triggered by drought and temperature stress. Nat. Clim. Change 3, 30-36.
- 43. Prestele, R., Alexander, P., Rounsevell, M.D.A., Arneth, A., Calvin, K., Doelman, J., Eitelberg, D.A., Engström, K., Fujimori, S., Hasegawa, T., et al. (2016). Hotspots of uncertainty in land-use and land-cover change projections: a global-scale model comparison. Global Change Biol. 22,
- 44. Seddon, N., Smith, A., Smith, P., Key, I., Chausson, A., Girardin, C., House, J., Srivastava, S., and Turner, B. (2021). Getting the message right on nature-based solutions to climate change. Global Change Biol. 27,
- 45. Schuiling, R.D., and Krijgsman, P. (2006). Enhanced weathering: An effective and cheap tool to sequester CO2. Clim. Change 74, 349-354.
- 46. Calabrese, S., Wild, B., Bertagni, M.B., Bourg, I.C., White, C., Aburto, F., Cipolla, G., Noto, L.V., and Porporato, A. (2022). Nano-to global-scale uncertainties in terrestrial enhanced weathering. Environ. Sci. Technol. 56, 15261-15272
- 47. Domke, G.M., Oswalt, S.N., Walters, B.F., and Morin, R.S. (2020). Tree planting has the potential to increase carbon sequestration capacity of forests in the United States. Proc. Natl. Acad. Sci. USA 117, 24649-24651.
- 48. Nolan, C.J., Field, C.B., and Mach, K.J. (2021). Constraints and enablers for increasing carbon storage in the terrestrial biosphere. Nat. Rev. Earth Environ. 2, 436-446.
- 49. Kuzyakov, Y. (2010). Priming effects: Interactions between living and dead organic matter. Soil Biol. Biochem. 42, 1363-1371.
- 50. Knutti, R., Sedláček, J., Sanderson, B.M., Lorenz, R., Fischer, E.M., and Eyring, V. (2017). A climate model projection weighting scheme accounting for performance and interdependence. Geophys. Res. Lett. 44, 1909-1918.
- 51. Ribes, A., Qasmi, S., and Gillett, N.P. (2021). Making climate projections conditional on historical observations. Sci. Adv. 7, eabc0671.
- 52. Konings, A.G., Bloom, A.A., Liu, J., Parazoo, N.C., Schimel, D.S., and Bowman, K.W. (2019). Global satellite-driven estimates of heterotrophic respiration. Biogeosciences 16, 2269-2284.
- 53. Franklin, O., Harrison, S.P., Dewar, R., Farrior, C.E., Brännström, Å., Dieckmann, U., Pietsch, S., Falster, D., Cramer, W., Loreau, M., et al. (2020). Organizing principles for vegetation dynamics. Nat. Plants 6, 444-453.
- 54. Wieder, W.R., Allison, S.D., Davidson, E.A., Georgiou, K., Hararuk, O., He, Y., Hopkins, F., Luo, Y., Smith, M.J., Sulman, B., et al. (2015). Explicitly representing soil microbial processes in Earth system models. Global Biogeochem. Cycles 29, 1782-1800.
- 55. Sulman, B.N., Moore, J.A.M., Abramoff, R., Averill, C., Kivlin, S., Georgiou, K., Sridhar, B., Hartman, M.D., Wang, G., Wieder, W.R., et al. (2018). Multiple models and experiments underscore large uncertainty in soil carbon dynamics. Biogeochemistry 141, 109-123.
- 56. Fatichi, S., Manzoni, S., Or, D., and Paschalis, A. (2019). A mechanistic model of microbially mediated soil biogeochemical processes: a reality check. Global Biogeochem. Cycles 33, 620-648.
- 57. Abramoff, R., Xu, X., Hartman, M., O'Brien, S., Feng, W., Davidson, E., Finzi, A., Moorhead, D., Schimel, J., Torn, M., and Mayes, M.A. (2018). The Millennial model: in search of measurable pools and transformations for modeling soil carbon in the new century. Biogeochemistry 137, 51-71.
- 58. Calabrese, S., Mohanty, B.P., and Malik, A.A. (2022). Soil microorganisms regulate extracellular enzyme production to maximize their growth rate. Biogeochemistry 158, 303-312.

Please cite this article in press as: Huang et al., Widespread temporal and spatial variability in net ecosystem productivity under climate change, One Earth (2024), https://doi.org/10.1016/j.oneear.2024.01.008





- 59. Raftery, A.E., Painter, I.S., and Volinsky, C.T. (2005). BMA: an R package for Bayesian model averaging. The Newsletter of the R Project 5, 2–8.
- 60. Song, X., Wang, D.Y., Li, F., and Zeng, X.D. (2021). Evaluating the performance of CMIP6 Earth system models in simulating global vegetation structure and distribution. Adv. Clim. Change Res. 12, 584-595.
- 61. Legendre, P. (2018). Imodel2: Model II regression. R Package v.1.7-3. [WWWdocument]. https://CRAN.R-project.org/package=Imodel2.
- 62. Huang, M., Ray, J., Hou, Z., Ren, H., Liu, Y., and Swiler, L. (2016). On the applicability of surrogate-based Markov chain Monte Carlo-Bayesian
- inversion to the Community Land Model: Case studies at flux tower sites. JGR. Atmospheres 121, 7548-7563.
- 63. Fer, I., Kelly, R., Moorcroft, P.R., Richardson, A.D., Cowdery, E.M., and Dietze, M.C. (2018). Linking big models to big data: efficient ecosystem model calibration through Bayesian model emulation. Biogeosciences 15, 5801-5830.
- 64. Liu, Y., He, N., Wen, X., Xu, L., Sun, X., Yu, G., Liang, L., and Schipper, L.A. (2018). The optimum temperature of soil microbial respiration: Patterns and controls. Soil Biol. Biochem. 121, 35-42.